An efficient threshold dynamics method for wetting on rough surfaces

Xianmin Xu[a], Dong Wang[b], Xiaoping Wang[c]

[a] *LSEC, Institute of Computational Mathematics and Scientific/Engineering Computing, NCMIS, AMSS, Chinese Academy of Sciences, Beijing 100190, China (xmxu@lsec.cc.ac.cn).*

[b] *Department of Mathematics, the Hong Kong University of Science and Technology, Clear Water Bay, Kowloon, Hong Kong, China. (dwangaf@connect.ust.hk).*

[c] *Department of Mathematics, the Hong Kong University of Science and Technology, Clear Water Bay, Kowloon, Hong Kong, China. (mawang@ust.hk).*

Abstract

A threshold dynamics method was developed by Merriman, Bence and Osher(MBO) to simulate the motion by mean curvature flow. The method has the advantage of being unconditionally stable and fast with the complexity only $O(N \log N)$, where N is the total number of grid points. The method has also been extended to problems with volume preservation. However, the generalization of the MBO type method to wetting problem with interface intersecting the boundary is not obvious because of lack of integral representation with heat kernel for general domain with boundary. We develop an efficient volume preserving threshold dynamics method for wetting on rough surfaces. The method is simple, stable with the complexity $O(N \log N)$ per time step and it is not sensitive to the inhomogeneity or roughness of the solid boundary.

Keywords: Threshold method, wetting, rough surface

1. Introduction

Wetting describes how a liquid drop stays and spreads on a solid surface. The most important quantity in wetting is the contact angle between the liquid surface and the solid surface[9]. When the solid surface is homogeneous, the contact angle for a static liquid drop is given by the famous Young's

equation,

$$\cos\theta_Y = \frac{\gamma_{SV} - \gamma_{SL}}{\gamma_{LV}}, \tag{1}$$

where γ_{SL}, γ_{SV} and γ_{LV} are the solid-liquid, solid-vapor and liquid-vapor surface energy tensions, respectively. θ_Y is the so-called Young's angle[34]. Mathematically, the Young's equation (1) can be derived by minimizing the total energy in the solid-liquid-vapor system. If we ignore the gravity, the total energy in the system is written as

$$\mathcal{E} = \gamma_{LV}|\Sigma_{LV}| + \gamma_{SL}|\Sigma_{SL}| + \gamma_{SV}|\Sigma_{SV}|, \tag{2}$$

where Σ_{LV}, Σ_{SL} and Σ_{SV} are respectively the liquid-vapor, solid-liquid and solid-vapor interfaces, and $|\cdot|$ denotes the area of interfaces. When the solid surface Γ is a homogeneous planar surface, under the condition that the volume of the droplet is fixed, the unique minimizer of the energy is a domain with a spherical surface in Ω, and the contact angle between the surface and the solid surface Γ is the Young's angle θ_Y[30].

The study of wetting and contact angle hysteresis on rough surfaces is of critical importance for many applications and has attracted much interest in physics and applied mathematics communities [24, 16, 2, 33, 12]. Numerical simulation of the wetting on rough surface is a challenging task. One not only needs to track the interface motion accurately, but also needs to deal with complicated boundary shapes and boundary conditions. There are many different types of numerical methods for interface and contact line problems, including front tracking method [31, 20], front capturing method using level-set function[35], the phase-field methods[11, 4], and some others[10].

An efficient threshold dynamics method was developed by Merriman, Bence and Osher(MBO) [21, 22] to simulate the motion by mean curvature flow, which is based on the observation that the level-set of the solution of a heat equation moves in normal direction with velocity equal to the mean curvature of level-set surface. The method alternately diffuses and sharpens characteristic functions for regions and is easy to implement and highly efficient. The method has also been extended to problems with volume preservation [27, 19] and to some high order geometric flow problems[14]. Recently, Esedoglu and Otto have extended the threshold dynamics method to the multi-phase problems with arbitrary surface tensions[13]. There have been many studies on the MBO threshold dynamics method, including more efficient implementations [26, 25] and the error analysis[3, 15, 6, 18].

The generalization of the MBO type method to wetting problem with interface intersecting with the boundary is not obvious because of lack of integral representation with heat kernel for general domain with boundary. In the original MBO scheme, when the interface doesn't intersect with the solid boundary, one can solve the heat equation efficiently on a rectangular domain with uniform grid using convolution of heat kernel with the initial condition [26, 25]. The convolution can be evaluated using fast Fourier transform(FFT) at $M \log(M)$ cost per time step where M is the total number of grid points. One way to generalize the MBO type method to wetting on solid surface is to solve the heat equation with a wetting boundary condition before the volume preserving thresholding. However, In this case, and in particular for the rough boundaries, the usual fast algorithms can not be applied easily.

In this paper, we aim to develop an efficient volume-preserving threshold dynamics method for wetting problems on rough surfaces. Our method is based on the approach of Esedoglu-Otto in [13]. The key idea is to extend the original domain with rough boundary to a regular cube and treat the solid part as another phase. In the thresholding step, the solid phase domain remains unchanged. We show that the algorithm has the total interface energy decaying property and our numerical results show that the equilibrium interface satisfies the Young's equation at the contact point. The advantage of the method is that it can be implemented efficiently on uniform mesh with fast algorithm (e.g. FFT) since the computational domain is rectangular and we can simulate wetting on rough boundary of any shape. We also introduce a fast algorithm for volume-preservation based on a quicksort algorithm and a time refinement scheme to improve the accuracy of the solution at contact line.

The outline of the paper is as follows. In Section 2, we first describe a MBO type threshold method for wetting problem. This is based on standard threshold method but less efficient due to the roughness or inhomogeneity of the solid boundary and the special boundary conditions there. In Section 3, we introduce a new threshold method which is simple, efficient and easy to implement. Several different modifications of the method are also discussed. In Section 4, we introduce a fast algorithm for volume conservation and time adaptivity technique to improve the accuracy of the contact line motion. In Section 5 and Section 6, we present some numerical examples of wetting on rough surfaces to demonstrate the efficiency of the new method.

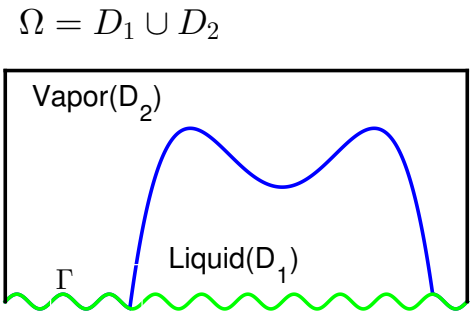

Figure 1: Wetting on a rough surface

2. A MBO type threshold method

We consider a wetting problem in a domain $\Omega \in \mathbb{R}^n$, $n = 2, 3$ (see Fig. 2). The solid surface Γ is part of the domain boundary $\partial\Omega$. Denote the liquid domain as $D_1 \subset \Omega$. For simplicity, we assume that $\partial D_1 \cap \partial\Omega \subset \Gamma$. The volume of the liquid drop is fixed that $|D_1| = V_0$. We denote $\Sigma_{LV} = \partial D_1 \cap \Omega$, $\Sigma_{SL} = \partial D_1 \cap \Gamma$ and $\Sigma_{SV} = \Gamma \subset \partial D_1$ as the liquid-vapor, the solid-liquid and the solid-vapor interfaces respectively. Then, the equilibrium configuration of the system is obtained by minimizing the total interface energy of the system, i.e.

$$\min_{|D_1|=V_0} \mathcal{E}(D_1) = \gamma_{LV}|\partial D_1 \cap \Omega| + \int_{\partial D_1 \cap \Gamma} \gamma_{SL}(x)\mathrm{d}s + \int_{\Gamma \setminus \partial D_1} \gamma_{SV}(x)\mathrm{d}s \qquad (3)$$

where the solid boundary Γ is rough and/or chemically inhomogeneous (i.e. $\gamma_{SL}(x)$ and $\gamma_{SV}(x)$ may depend on x).

To solve the problem (3) numerically, it is convenient to use a diffuse interface model to approximate the sharp interface energy. Suppose φ is a phase-field function, such that $D_1 = \{\varphi < 0\}$ represents the liquid domain, $\{\varphi > 0\}$ represents the liquid domain and $\Sigma_{LV} = \{\varphi = 0\}$ is the liquid-vapor interface. The total energy (2) can be approximated by

$$\mathcal{E}_\varepsilon^{ph}(\varphi) = \int_\Omega \varepsilon|\nabla\varphi|^2 + \frac{f(\varphi)}{\varepsilon}\mathrm{d}\mathbf{x} + \int_\Gamma \gamma(x,\varphi)\mathrm{d}s, \qquad (4)$$

where ε is a small parameter representing interface thickness, $f(\varphi) = \frac{(1-\varphi^2)^2}{4}$ is a double-well function and

$$\gamma(\varphi) = \frac{\tilde{\gamma}_{SV}(x) + \tilde{\gamma}_{SL}(x)}{2} + \frac{\tilde{\gamma}_{SV}(x) - \tilde{\gamma}_{SL}(x)}{4}(3\varphi - \varphi^3).$$

It can be proved that when ε goes to zero, after a scaling, the energy in (4) converges to that in (2)[32]. Therefore, the problem (3) can be approximated by minimizing the total energy $\mathcal{E}_\varepsilon^{ph}$ under the volume constraint $\int_\Omega(\varphi - 1)/2 \mathrm{d}\mathbf{x} = V_0$.

The H^{-1} gradient flow of the energy functional (4) will lead to a Cahn-Hilliard equation with contact angle boundary condition[8]. Alternatively, the L^2 gradient flow will lead to a modified Allen-Cahn equation:

$$\begin{cases} \varphi_t = \varepsilon\Delta\varphi - \frac{f'(\varphi)}{\varepsilon} + \delta & \text{in } \Omega; \\ \frac{\partial\varphi}{\partial n} + \gamma'(x,\varphi) = 0, & \text{on } \Gamma; \\ \varphi(x) = -1, & \text{on } \partial\Omega \setminus \Gamma, \\ \int_\Omega \frac{\varphi-1}{2} \mathrm{d}\mathbf{x} = V_0. \end{cases} \tag{5}$$

Here δ is a Lagrangian multiplier for the volume constraint.

Motivated by the MBO approach in [21], a threshold dynamics scheme can be derived easily based on a splitting method for (5). Assume we have a solution φ^k at the k-th time step, we can first solve the heat equation

$$\begin{cases} \bar{\varphi}_t = \varepsilon\Delta\bar{\varphi} & \text{in } \Omega. \\ \frac{\partial\bar{\varphi}}{\partial n} + \gamma'(x,\bar{\varphi}) = 0, & \text{on } \Gamma, \\ \bar{\varphi}(x,0) = \bar{\varphi}^k, \end{cases} \tag{6}$$

until some time δt_1 and then solve

$$\begin{cases} \varphi_t = -\frac{f'(\varphi)}{\varepsilon} \\ \varphi(x,0) = \bar{\varphi}(x,\delta t_1) \end{cases} \tag{7}$$

until some time δt_2 and set $\varphi^{k+1} = \varphi(x,\delta t_2)$. It is easy to see that when $\delta t_2/\varepsilon$ is large enough, solving the second equation (7) is reduced to a threshold step that

$$\varphi(x,\delta t_2) \approx \begin{cases} -1 & \text{if } \varphi(x,0) < 0; \\ 1 & \text{if } \varphi(x,0) > 0. \end{cases} \tag{8}$$

This implies that, in the next step we can use a piecewise constant function φ^{k+1} as the initial condition to solve (6). In this case, the solution of (5) will be obtained by repeatedly solving (6) and the threshold step (8). This leads to the following MBO scheme for wetting problem:

A MBO threshold dynamics scheme for the wetting problem

Step 0. *Given an initial domain $D_1^0 \subset \Omega$ such that $|D_1^0| = V_0$. Set a tolerance parameter $\varepsilon > 0$.*

Step 1. *For any k, we first solve the heat equation*

$$\begin{cases} \varphi_t = \varepsilon \Delta \varphi & \text{in } \Omega. \\ \frac{\partial \phi}{\partial n} + \gamma'(x, \varphi) = 0, & \text{on } \Gamma, \\ \varphi(x, 0) = \chi_{D_1^k}, \end{cases} \tag{9}$$

until some time δt.

Step 2. *Determine a new D_1^{k+1} by threshold method*

$$D_1^{n+1} = \{x : \varphi(x, \delta t) < \frac{1}{2} + \delta\}.$$

Here δ is chosen to make sure the volume $|D_1^{k+1}| = V_0$.

Step 3. *If $|D_1^k - D_1^{k+1}| < \varepsilon$, step; otherwise, set $k = k+1$ and go back to Step 1.*

In the original MBO scheme, when the interface doesn't intersect with the solid boundary, one can solve the heat equation efficiently on a uniform grid using convolution of heat kernel with the initial condition [26, 25]. The convolution can be evaluated using fast Fourier transform(FFT) at $M \log(M)$ cost per time step where M is the total number of grid points. However, when interface intersect with the solid boundary, one needs to solve the heat equation with the wetting boundary condition as in (9). In this case, and in particular for the rough boundaries, the usual fast algorithms can not be applied to solve (9). In the next section, we will introduce a new threshold dynamic method.

3. A new threshold dynamics method for wetting problem

In this section, we introduce a new threshold method which is motivated by a recent work by Esedoglu and Otto[13]. The main idea is to extend the fluid domain Ω to a larger domain, which contains the solid phase. In the extended domain, the interface energies between different phases in (3) can be approximated by a convolution of characteristic functions and a Guassian kernel(see details below). We then derive a simple scheme to minimize the new energy functional with the constraint that the solid phase does not change and the volume of the liquid phase is preserved. The scheme leads to a new threshold method for wetting problem.

3.1. The representation of the interface energies in an extended domain

In the following, we let $D_1, D_2 \subset \Omega$ be the liquid and the vapor phases, respectively. Let $\Sigma_{LV} = \partial D_1 \cap \partial D_2$ be the liquid-vapor interface. In [1, 23], it is shown that when $\delta t \ll 1$, the area of Σ_{LV} can be approximated by

$$|\Sigma_{LV}| \approx \frac{1}{\sqrt{\delta t}} \int \chi_{D_1} G_{\delta t} * \chi_{D_2} \mathrm{d}\mathbf{x}. \tag{10}$$

where χ_{D_i} is the characteristic function of D_i and

$$G_{\delta t}(\mathbf{x}) = \frac{1}{(4\pi\delta t)^{n/2}} \exp(-\frac{|\mathbf{x}|^2}{4\delta t})$$

is the Guassian kernel.

In the total energy (3), the second and third terms are surface energies defined on the solid surface Γ. They are the solid-liquid interfacial energy term on $\Sigma_{SL} = \partial D_1 \cap \Gamma$ and the solid-vapor interfacial energy term on $\Sigma_{SV} = \partial D_2 \cap \Gamma$. To approximate the two terms using Guassian kernel, we extend the domain Ω beyond Γ(see Figure 3.1). The extended domain is $\tilde{\Omega} = \Omega \cup D_3$ where D_3 is the solid region. Then, the solid surface is $\Gamma = \partial\Omega \cap \partial D_3$, the solid-liquid interface is $\Sigma_{SL} = \partial D_1 \cap \partial D_3$ and the solid-vapor interface is $\Sigma_{SV} = \partial D_2 \cap \partial D_3$. Similar to (10), the total energy $\mathcal{E}$ in (3) can be approximated by

$$\begin{aligned}
&\mathcal{E}^{\delta t}(\chi_{D_1}, \chi_{D_2}) = \\
&\frac{\gamma_{LV}}{\sqrt{\delta t}} \int_{\tilde{\Omega}} \chi_{D_1} G_{\delta t} * \chi_{D_2} \mathrm{d}\mathbf{x} + \frac{\gamma_{SL}}{\sqrt{\delta t}} \int_{\tilde{\Omega}} \chi_{D_1} G_{\delta t} * \chi_{D_3} \mathrm{d}\mathbf{x} + \frac{\gamma_{SV}}{\sqrt{\delta t}} \int_{\tilde{\Omega}} \chi_{D_2} G_{\delta t} * \chi_{D_3} \mathrm{d}\mathbf{x}.
\end{aligned} \tag{11}$$

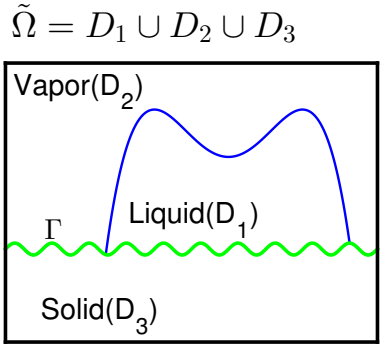

Figure 2: Expand the domain beyond to $\tilde{\Omega} = \Omega \cup D_3$

For simplicity, we assume γ_{SL} and γ_{SV} are constants throughout this section. The analysis and the algorithms can be easily generalized to cases when they are not homogeneous. In the next section, we will apply the method to a chemically patterned surface where γ_{SL} and γ_{SV} are piecewise constant functions.

Denote $u_1 = \chi_{D_1}$ and $u_2 = \chi_{D_2}$. We define an admissible set

$$\mathcal{B} = \{(u_1, u_2) \in BV(\Omega) \mid u_i(x) = 0, 1, \text{ and } u_1(x) + u_2(x) = 1, \ a.e.\ x \in \Omega, \int_\Omega u_1 d\mathbf{x} = V_0\} \tag{12}$$

The wetting problem (3) can be approximated by

$$\min_{(u_1,u_2)\in\mathcal{B}} \mathcal{E}^{\delta t}(u_1, u_2). \tag{13}$$

This is a nonconvex minimization problem since $\mathcal{B}$ is not a convex set. The Γ-convergence of the problem (13) to (3) can be proved in a similar way as in [13].

3.2. Derivation of the threshold dynamics method

We will derive the threshold method for the problem (13). We first show that the nonconvex problem (13) can be relaxed to an equivalent convex

problem. Then we derive a threshold method for the convex problem. The relaxed problem is given by

$$\min_{(u_1,u_2)\in\mathcal{K}} \mathcal{E}^{\delta t}(u_1,u_2). \tag{14}$$

where $\mathcal{K}$ is the convex hull of the admissible set $\mathcal{B}$:

$$\mathcal{K}=\{(u_1,u_2)\in BV(\Omega)|0\le u_i\le 1, u_1(x)+u_2(x)=1,\ a.e.\ x\in\Omega, \int_\Omega u_1 \mathrm{d}\mathbf{x}=V_0\}. \tag{15}$$

The following lemma shows that the relaxed problem (14) is equivalent to the original problem (13). For convenience later, we prove the result for a slightly more general problem with an extra linear functional term $\mathcal{L}(u_1,u_2)$.

Lemma 3.1. *For any given $\alpha,\beta\ge 0$ and any linear functional $\mathcal{L}(u_1,u_2)$, we have*

$$\min_{(u_1,u_2)\in\mathcal{K}}(\alpha\mathcal{E}^{\delta t}(u_1,u_2)+\beta\mathcal{L}(u_1,u_2))=\min_{(u_1,u_2)\in\mathcal{B}}(\alpha\mathcal{E}^{\delta t}(u_1,u_2)+\beta\mathcal{L}(u_1,u_2)).$$

Proof. Let $(\tilde{u}_1,\tilde{u}_2)\in\mathcal{K}$ be a minimizer of the functional

$$\alpha\mathcal{E}^{\delta t}(u_1,u_2)+\beta\mathcal{L}(u_1,u_2).$$

Since $\mathcal{B}\subset\mathcal{K}$, we have

$$\begin{aligned}\alpha\mathcal{E}^{\delta t}(\tilde{u}_1,\tilde{u}_2)+\beta\mathcal{L}(\tilde{u}_1,\tilde{u}_2) &= \min_{(u_1,u_2)\in\mathcal{K}} \alpha\mathcal{E}^{\delta t}(u_1,u_2)+\beta\mathcal{L}(u_1,u_2)\\ &\le \min_{(u_1,u_2)\in\mathcal{B}} \alpha\mathcal{E}^{\delta t}(u_1,u_2)+\beta\mathcal{L}(u_1,u_2).\end{aligned}$$

Therefore, we need only to prove that $(\tilde{u}_1,\tilde{u}_2)\in\mathcal{B}$.

The claim is trivial when $\alpha=0$, since the minimizer of a linear functional in a convex set must belong to the boundary of the set. When $\alpha>0$, we prove by contradictions. If $(\tilde{u}_1,\tilde{u}_2)\notin\mathcal{B}$, there is a set $A\in\Omega$ and a constant $0<C_0<\frac{1}{2}$, such that $|A|>0$ and

$$0<C_0<\tilde{u}_1(x),\tilde{u}_2(x)<1-C_0,\quad \text{for all } x\in A.$$

We divide A into two sets $A=A_1\cup A_2$ such that $A_1\cap A_2=\emptyset$ and $|A_1|=|A_2|=|A|/2$. Denote $u_1^t=\tilde{u}_1+t\chi_{A_1}-t\chi_{A_2}$ and $u_2^t=\tilde{u}_2-t\chi_{A_1}+t\chi_{A_2}$. When $0<t<C_0$, we have $0<u_1^t,u_2^t<1$ and

$$u_1^t+u_2^t=\tilde{u}_1+\tilde{u}_2=1,\ \text{and}\ \int_\Omega u_1^t\mathrm{d}\mathbf{x}=\int_\Omega\tilde{u}_1\mathrm{d}\mathbf{x}=V_0.$$

This implies that $(u_1^t, u_2^t) \in \mathcal{K}$. Furthermore, direct computation gives,

$$\begin{aligned}
\frac{d^2}{dt^2}(\alpha\mathcal{E}^{\delta t}(u_1^t, u_2^t) + \beta\mathcal{L}(u_1^t, u_2^t)) &= \frac{1}{\sqrt{\delta t}}\int_{\tilde{\Omega}} \frac{d}{dt}u_1^t G_{\delta t} * \frac{d}{dt}u_2^t \mathrm{d}\mathbf{x} \\
&= \frac{1}{\sqrt{\delta t}}\int_{\tilde{\Omega}} (\chi_{A_1} - \chi_{A_2}) G_{\delta t} * (\chi_{A_2} - \chi_{A_1}) \mathrm{d}\mathbf{x} \\
&= -\frac{1}{\sqrt{\delta t}}\int_{\tilde{\Omega}} (\chi_{A_1} - \chi_{A_2}) G_{\delta t} * (\chi_{A_1} - \chi_{A_2}) \mathrm{d}\mathbf{x} \\
&< 0.
\end{aligned}$$

The functional is concave on the point $(\tilde{u}_1, \tilde{u}_2)$. Thus, $(\tilde{u}_1, \tilde{u}_2)$ can not be a minimizer of the functional. This contradicts the assumption. □

The above lemma implies that we can solve the relaxed problem (14) instead of the original one (13). In the following, we show that the problem can be solved iteratively by a threshold method.

Suppose we solve the problem (14) by an iterative method. In the k step, we have an approximated solution (u_1^k, u_2^k). The energy functional $\mathcal{E}^{\delta t}(u_1, u_2)$ can be linearized near the point (u_1^k, u_2^k):

$$\mathcal{E}^{\delta t}(u_1, u_2) \approx \mathcal{E}^{\delta t}(u_1^k, u_2^k) + \hat{\mathcal{L}}(u_1 - u_1^k, u_2 - u_2^k, u_1^k, u_2^k) + h.o.t.$$

with

$$\begin{aligned}
&\hat{\mathcal{L}}(u_1, u_2, u_1^k, u_2^k) = \\
&\frac{1}{\sqrt{\delta t}}\left(\int_{\tilde{\Omega}} u_1 G_{\delta t} * (\gamma_{LV} u_2^k + \gamma_{SL}\chi_{D_3})\mathrm{d}\mathbf{x} + \int_{\tilde{\Omega}} u_2 G_{\delta t} * (\gamma_{LV} u_1^k + \gamma_{SV}\chi_{D_3})\mathrm{d}\mathbf{x}\right).
\end{aligned} \tag{16}$$

Then we minimize the linearized functional:

$$\min_{(u_1,u_2)\in\mathcal{K}} \hat{\mathcal{L}}(u_1, u_2, u_1^k, u_2^k) \tag{17}$$

and set the solution to be (u_1^{k+1}, u_2^{k+1}). By Lemma 3.1, the solution of (17) is in $\mathcal{B}$. In other words, u_1^{k+1} and u_2^{k+1} are characteristic functions of some proper sets D_1^{k+1} and D_2^{k+1} such that $|D_1^{k+1}| = V_0$.

The following lemma shows that the minimizing problem (17) is solved by a simple thresholding approach.

Lemma 3.2. *Denote*

$$\phi_1 = \frac{1}{\sqrt{\delta t}} G_{\delta t} * (\gamma_{LV} u_2^k + \gamma_{SL} \chi_{D_3}),\ \ \phi_2 = \frac{1}{\sqrt{\delta t}} G_{\delta t} * (\gamma_{LV} u_1^k + \gamma_{SV} \chi_{D_3}). \quad (18)$$

Let

$$D_1^{k+1} = \{x \in \Omega |\ \phi_1 < \phi_2 + \delta\} \quad (19)$$

for some δ such that $|D_1^{k+1}| = V_0$. Define $D_2^{k+1} = \Omega \backslash D_1^{k+1}$. Then $(u_1^{k+1}, u_2^{k+1}) = (\chi_{D_1^{k+1}}, \chi_{D_2^{k+1}})$ is a solution of (17).

Proof. By Lemma 3.1, we need only to prove

$$\hat{\mathcal{L}}(u_1^{k+1}, u_2^{k+1}, u_1^k, u_2^k) \leq \hat{\mathcal{L}}(u_1, u_2, u_1^k, u_2^k), \quad (20)$$

for all $(u_1, u_2) \in \mathcal{B}$.

For each $(u_1, u_2) \in \mathcal{B}$, we know $u_1 = \chi_{\hat{D}_1}$ and $u_2 = \chi_{\hat{D}_2}$ for some open set $\hat{D}_1$, $\hat{D}_2$ in Ω, such that $\hat{D}_1 \cap \hat{D}_2 = \emptyset$, $\hat{D}_1 \cup \hat{D}_2 = \Omega$ and $|\hat{D}_1| = V_0$. Let $A_1 = \hat{D}_1 \setminus D_1^{k+1} = D_2^{k+1} \setminus \hat{D}_2$ and $A_2 = \hat{D}_2 \setminus D_2^{k+1} = D_1^{k+1} \setminus \hat{D}_1$. We must have $|A_1| = |A_2|$ due to the volume conversation property. Since $A_1 \subset D_2^{k+1}$, we have

$$\phi_1(x) \geq \phi_2(x) + \delta, \quad \forall x \in A_1.$$

Similarly, since $A_2 \in D_1^{k+1}$, we have

$$\phi_1(x) < \phi_2(x) + \delta, \quad \forall x \in A_2.$$

Therefore, we have

$$\begin{aligned}
&\hat{\mathcal{L}}(u_1^{k+1}, u_2^{k+1}, u_1^k, u_2^k) - \hat{\mathcal{L}}(u_1, u_2, u_1^k, u_2^k) \\
=& \int_{\tilde{\Omega}} (u_1^{k+1} - u_1)\phi_1 + (u_2^{k+1} - u_2)\phi_2 \mathrm{d}\mathbf{x} \\
=& -\int_{A_1} \phi_1 \mathrm{d}\mathbf{x} + \int_{A_2} \phi_1 \mathrm{d}\mathbf{x} - \int_{A_2} \phi_2 \mathrm{d}\mathbf{x} + \int_{A_1} \phi_2 \mathrm{d}\mathbf{x} \\
=& \int_{A_1} (\phi_2 - \phi_1)\mathrm{d}\mathbf{x} + \int_{A_2} (\phi_1 - \phi_2)\mathrm{d}\mathbf{x} \\
\leq& -\delta \int_{A_1} \mathrm{d}\mathbf{x} + \delta \int_{A_2} \mathrm{d}\mathbf{x} = 0.
\end{aligned}$$

This finishes the proof. □

We are led to the following threshold dynamics algorithm:

Algorithm I:

Step 0. *Given initial $D_1^0, D_2^0 \subset \Omega$, such that $D_1^0 \cap D_2^0 = \emptyset$, $D_1^0 \cup D_2^0 = \Omega$ and $|D_1^0| = V_0$. Set a tolerance parameter $\varepsilon > 0$.*

Step 1. *For given set (D_1^k, D_2^k), we define two functions*

$$\phi_1 = \frac{1}{\sqrt{\delta t}} G_{\delta t} * (\gamma_{LV}\chi_{D_2^k} + \gamma_{SL}\chi_{D_3}),\ \phi_2 = \frac{1}{\sqrt{\delta t}} G_{\delta t} * (\gamma_{LV}\chi_{D_1^k} + \gamma_{SV}\chi_{D_3}). \tag{21}$$

Step 2. *Find a δ so that the set*

$$\tilde{D}_1^\delta = \{x \in \Omega | \phi_1 < \phi_2 + \delta.\} \tag{22}$$

satisfies $|\tilde{D}_1^\delta| = V_0$. Denote $D_1^{k+1} = \tilde{D}_1^\delta$ and $D_2^{k+1} = \Omega \setminus D_1^{k+1}$.

Step 3. *If $|D_1^k - D_1^{k+1}| \le \varepsilon$, stop. Otherwise, go back to Step 1.*

Remark 3.1. *The method is simple and easy to implement.*

(1). We can always extend Ω to a cubic domain $\tilde{\Omega}$, since the only constraint of the extension is $D_1 \in \tilde{\Omega}$ and $|D_1| = V_0$. For the cube domain, the convolution in (21) *can be computed by fast algorithms (e.g. the FFT).*

(2). To keep the volume of the liquid phase unchanged, we need to find a proper δ in Step 2. This can be done by using a bisection method or a decent method, as shown in [27] for mean curvature flow. In the next section, we will give a simpler technique to determine δ, which is more efficient than existing methods.

(3). The above derivation of the thresholding method for wetting problem can be easily generalized to a multiphase system with wetting boundary conditions, e.g. the three-phase system[28], in the same line as that in Esedoglu and Otto[13]. For each phase, we need to compute a function similar to that in (21).

3.3. A simplified algorithm for the two phase problem

In case of two phase problem, the Algorithm I can be simplified as follows. Noticing that $u_1 + u_2 = 1$ in Ω, we actually have only one unknown u_1 in (11). Define

$$\mathcal{K}_1 = \{u \in BV(\Omega) | 0 \le u \le 1,\ a.e.\ x \in \Omega, \int_\Omega u d\mathbf{x} = V_0\}.$$

It is easy to see that (14) can be rewritten as

$$\begin{aligned}\min_{u_1\in\mathcal{K}_1}\tilde{\mathcal{E}}^{\delta t}(u_1) =& -\gamma_{LV}\int_{\tilde{\Omega}} u_1 G_{\delta t} * u_1 \mathrm{d}\mathbf{x} + \gamma_{LV}\int_{\tilde{\Omega}} u_1 G_{\delta} * \chi_{\Omega}\mathrm{d}\mathbf{x} \\ &+ \int_{\tilde{\Omega}}(\gamma_{SL}-\gamma_{SV})u_1 G_{\delta t} * \chi_{D_3}\mathrm{d}\mathbf{x} + \int_{\tilde{\Omega}}\gamma_{SV}\chi_{\Omega} G_{\delta t} * \chi_{D_3}\mathrm{d}\mathbf{x}.\end{aligned} \tag{23}$$

Suppose we solve the problem by an iterative method. For any given u_1^k, we could linearize the functional as

$$\tilde{\mathcal{E}}^{\delta t}(u_1) = \tilde{\mathcal{E}}^{\delta t}(u_1^k) + \tilde{\mathcal{L}}(u - u_1^k, u_1^k) + h.o.t.$$

with

$$\begin{aligned}\tilde{\mathcal{L}}(u, u_1^k) =& -2\gamma_{LV}\int_{\tilde{\Omega}} u_1 G_{\delta t} * u_1^k \mathrm{d}\mathbf{x} + \gamma_{LV}\int_{\tilde{\Omega}} u_1 G_{\delta} * \chi_{\Omega}\mathrm{d}\mathbf{x} \\ &+ \int_{\tilde{\Omega}}(\gamma_{SL}-\gamma_{SV})u_1 G_{\delta t} * \chi_{D_3}\mathrm{d}\mathbf{x} \\ =&\gamma_{LV}\int_{\tilde{\Omega}} u_1 G_{\delta t} * (u_2^k - u_1^k)\mathrm{d}\mathbf{x} + \int_{\tilde{\Omega}}(\gamma_{SL}-\gamma_{SV})u_1 G_{\delta t} * \chi_{D_3}\mathrm{d}\mathbf{x} \\ =&\gamma_{LV}\int_{\tilde{\Omega}} u_1 G_{\delta t} * (u_2^k - u_1^k - \cos\theta_Y \chi_{D_3})\mathrm{d}\mathbf{x}.\end{aligned} \tag{24}$$

Here we use the Young's equation $\gamma_{LV}\cos\theta_Y = \gamma_{SV} - \gamma_{SL}$.

As in the previous subsection, for the linearized functional (24), we can prove the following result. The proof is similar to that for Lemma (3.2).

Lemma 3.3. *Suppose $u_1^k = \chi_{D_1^k}$ for some set $D_1^k \subset \Omega$ and $D_2^k = \Omega \setminus D_1^k$. Denote*

$$\phi = \frac{\gamma_{LV}}{\sqrt{\delta t}} G_{\delta t} * (\chi_{D_2^k} - \chi_{D_1^k} - \cos(\theta_Y)\chi_{D_3}),$$

Let $\tilde{D}_1^{\delta} = \{x \in \Omega \mid \phi < \delta\}$, with some δ such that $|D_1^{k+1}| = V_0$. Then $u_1^{k+1} = \chi_{D_1^{k+1}}$ is a minimizer of $\tilde{\mathcal{L}}(u, u_1^k)$ in $\mathcal{K}_1$.

This will lead to the following algorithm.

Algorithm II:

Step 0. *Given initial $D_1^0 \subset \Omega$, such that $|D_1^0| = V_0$. Set a tolerance parameter $\varepsilon > 0$.*

Step 1. *For given set D_1^k, set $D_2^k = \Omega \setminus D_1^k$. We define a function*

$$\phi = \frac{\gamma_{LV}}{\sqrt{\delta t}} G_{\delta t} * (\chi_{D_2^k} - \chi_{D_1^k} - \cos(\theta_Y)\chi_{D_3}), \tag{25}$$

Step 2. *Find a $\delta \in (-1, 1)$, so that the set*

$$\tilde{D}_1^\delta = \{x \in \Omega \mid \phi < \delta.\} \tag{26}$$

satisfying $|\tilde{D}_1^{\delta_0}| = V_0$. Denote $D_1^{k+1} = \tilde{D}_1^{\delta_0}$.

Step 3. *If $|D_1^k - D_1^{k+1}| \leq \varepsilon$, stop. Otherwise, go back to Step 1.*

The following proposition shows that Algorithm I and Algorithm II are equivalent to each other.

Proposition 3.1. *For any domain $(D_1^k, D_2^k) \in \mathcal{B}$, after one iteration, Algorithm 2 and Algorithm 3 generate the same (D_1^{k+1}, D_2^{k+1}).*

Proof. We need only consider the threshold equation (22) and (26). Direct computations give

$$\begin{aligned}
\phi_1 - \phi_2 =& \frac{1}{\sqrt{\delta t}} G_{\delta t} * (\gamma_{LV}\chi_{D_2^k} + \gamma_{SL}\chi_{D_3}) - \frac{1}{\sqrt{\delta t}} G_{\delta t} * (\gamma_{LV}\chi_{D_1^k} + \gamma_{SV}\chi_{D_3}) \\
=& \frac{1}{\sqrt{\delta t}} G_{\delta t} * \Big(\gamma_{LV}(\chi_{D_2^k} - \chi_{D_1^k}) + (\gamma_{SL} - \gamma_{SV})\chi_{D_3}\Big) \\
=& \frac{\gamma_{LV}}{\sqrt{\delta t}} G_{\delta t} * (\chi_{D_2^k} - \chi_{D_1^k} - \cos\theta_Y \chi_{D_3}) = \phi.
\end{aligned}$$

In the last equation, we use the Young's equation. Therefore, the threshold step by (22) is equivalent to that by (26). This completes the proof. □

3.4. Stability analysis

In this subsection, we will show that the two algorithms above are stable, in the sense that the total energy of $\mathcal{E}^{\delta t}$ always decrease in the algorithm for any $\delta t > 0$. We have the following Theorem.

Theorem 3.1. *Denote $(u_1^k, u_2^k) = (\chi_{D_1^k}, \chi_{D_2^k})$, $k = 0, 1, 2, ...$, obtained in Algorithm I (or Algorithm II), we have*

$$\mathcal{E}^{\delta t}(u_1^{k+1}, u_2^{k+1}) \leq \mathcal{E}^{\delta t}(u_1^k, u_2^k), \tag{27}$$

for all $\delta t > 0$.

Proof. By Proposition 3.1, we need only to prove the Theorem for Algorithm I. By the definition of the linearization $\hat{\mathcal{L}}$ and Lemma (3.2), we know

$$\begin{aligned}
&\mathcal{E}^{\delta t}(u_1^k, u_2^k) + \frac{\gamma_{LV}}{\sqrt{\delta t}} \int_{\tilde{\Omega}} u_1^k G_{\delta t} * u_2^k \mathrm{d}\mathbf{x} = \hat{\mathcal{L}}(u_1^k, u_2^k, u_1^k, u_2^k) \\
&\geq \mathcal{L}(u_1^{k+1}, u_2^{k+1}, u_1^k, u_2^k) = \mathcal{E}^{\delta t}(u_1^{k+1}, u_2^{k+1}) \\
&\quad + \frac{\gamma_{LV}}{\sqrt{\delta t}} \left(\int_{\tilde{\Omega}} u_1^{k+1} G_{\delta t} * u_2^k \mathrm{d}\mathbf{x} + \int_{\tilde{\Omega}} u_2^{k+1} G_{\delta t} * u_1^k \mathrm{d}\mathbf{x} - \int_{\tilde{\Omega}} u_1^{k+1} G_{\delta t} * u_2^{k+1} \mathrm{d}\mathbf{x} \right).
\end{aligned}$$

This leads to

$$\mathcal{E}^{\delta t}(u_1^k, u_2^k) \geq \mathcal{E}^{\delta t}(u_1^{k+1}, u_2^{k+1}) + I, \tag{28}$$

with

$$\begin{aligned}
I = \frac{\gamma_{LV}}{\sqrt{\delta t}} \Big(& \int_{\tilde{\Omega}} u_1^{k+1} G_{\delta t} * u_2^k \mathrm{d}\mathbf{x} + \int_{\tilde{\Omega}} u_2^{k+1} G_{\delta t} * u_1^k \mathrm{d}\mathbf{x} \\
& - \int_{\tilde{\Omega}} u_1^{k+1} G_{\delta t} * u_2^{k+1} \mathrm{d}\mathbf{x} - \int_{\tilde{\Omega}} u_1^k G_{\delta t} * u_2^k \mathrm{d}\mathbf{x} \Big) \\
= -\frac{\gamma_{LV}}{\sqrt{\delta t}} & \int_{\tilde{\Omega}} (u_1^{k+1} - u_1^k) G_{\delta t} * (u_2^{k+1} - u_2^k) \mathrm{d}\mathbf{x}.
\end{aligned}$$

Using the fact that $u_1^k + u_2^k = u_1^{k+1} + u_2^{k+1}$,we have

$$I = \frac{\gamma_{LV}}{\sqrt{\delta t}} \int_{\tilde{\Omega}} (u_1^{k+1} - u_1^k) G_{\delta t} * (u_1^{k+1} - u_1^k) \mathrm{d}\mathbf{x} \geq 0.$$

This inequality together with (28) implies (27). □

The stability result does not mean that we can choose any large parameter δt in the algorithm, since the choice of δt also affect the accuracy of the approximation of $\mathcal{E}^{\delta t}$ to the energy $\mathcal{E}$ in (3).

4. Numerical implementation and accuracy check

In this section, we will introduce several techniques used to implemented the algorithm efficiently.

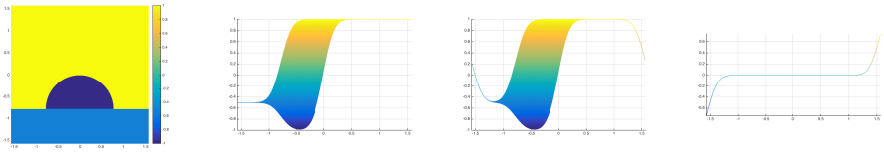

Figure 3: From left to right: 1. The initial condition defined by the charecteristic function of some domains. 2. The X-Z plane of the convolution between heat kernel and initial condition calculated by extending the domain by reflection (i.e. extend $[-\frac{\pi}{2}, \frac{\pi}{2}] \times [-\frac{\pi}{2}, \frac{\pi}{2}]$ to $[-\frac{\pi}{2}, \frac{3\pi}{2}] \times [-\frac{\pi}{2}, \frac{3\pi}{2}]$). 3. The X-Z plane of the convolution between heat kernel and initial condition calculated without extending the domain. 4. The error between the second figure and third figure.

4.1. Calculation of convolution

In Algorithm I, we need to calculate the two convolutions $G_{\delta t} * (\gamma_{LV}\chi_{D_2^k} + \gamma_{SL}\chi_{D_3})$ and $G_{\delta t} * (\gamma_{LV}\chi_{D_1^k} + \gamma_{SV}\chi_{D_3})$ on an extended domain $\tilde{\Omega}$ which we can always choose to be a rectangular domain. In this case, it is very efficient to used FFT to calculate the convolutions when the functions are periodic. To calculate convolutions for non-periodic functions, we can further extend the domain by reflection so that the functions are periodic on the extended domain. In our simulation, the characteristic function (e.g.$\gamma_{LV}\chi_{D_2^k} + \gamma_{SL}\chi_{D_3}$) are not periodic. However, since the heat kernel $G_{\delta t}$ decays exponentially fast and is negligibly small when $|x| > 10\sqrt{t}$. When we calculate the convolution, each target points will only be affected by a few neighboring points. Hence, if we apply FFT without extending the computational domain, we will only have some error near the boundary of computation domain (See Fig.3). When the dynamic interface is far away from the boundary of computational domain It is easy to see that after thresholding step, there is no difference between the solutions calculated with or without the extension of domain. Therefore, in our calculation, we always directly apply FFT without extending the computational domain.

4.2. A fast algorithm for volume conservation

In Step 2 of Algorithm I, we need to enforce the volume conservation. This is achived by shifting the thresholding level by a δ as in (22). The usual way to find δ by some iteration methods (e.g. bisection method, Newton method, fixed point iteration, see [27]). However, these iterative methods are quite sensitive to the initial guess. In this part, we will introduce a direct

and more efficient scheme to find a proper δ. If we consider uniform mesh (in two dimensions) and denote the mesh size as dx, the volume of a domain can be approximated by $V_0 \approx M \times dx^2$ (with first order accuracy). For our purpose, what we need to do in Step 2 is to find a threshold $\delta(M)$ such that there are M grid values of $\phi_1 - \phi_2$ which are less than δ. Since we have the values of $\phi_1 - \phi_2$ at each grid point, we can use the quicksort algorithm (available in Matlab)[17] to sort the values in ascending order in a list $\mathcal{S}$. We then choose the threshold value δ to be the average of the M^{th} value and $M + 1^{th}$ value in the ordered list $\mathcal{S}$, i.e. $\delta = \frac{\mathcal{S}(M)+\mathcal{S}(M+1)}{2}$, where $\mathcal{S}(M)$ is the M-th variable in the list. The scheme is summaried as the following:

A fast scheme for volume conservation

Step 0. *Set V_0 as the volume should be preserved and M as the integer part of V_0/dx^2*

Step 1. *Use quicksort algorithm to sort $\phi_1 - \phi_2$, which is defined in step 2 in Algorithm 2, in ascending order in a list $\mathcal{S}$.*

Step 2. *Set $\delta = \frac{\mathcal{S}(M)+\mathcal{S}(M+1)}{2}$*

In summary, the computational complexity to find δ is $O(Nlog(N))$ when we choose the quicksort algorithm. It is straightforward to see that this scheme will get the same δ as the iterative scheme proposed by Ruuth[27] (with first order accuracy). However, our scheme requires much less computational cost.

4.3. An adaptive scheme in time

For any given space meshes, the only parameter in Algorithm I is "the time step" δt. Based on the argument in Merriman, Bence and Osher[21], there are two requirements for the choice of δt: the first one is that δt should be small enough so that the approximation for the energy is accurate enough and the second is that δt should be also large enough so that the boundary curve moves at least one grid cell on the spatial grid (otherwise the interface would not move after the thresholding step), that is, $\delta t \gg \frac{\delta x}{\kappa}$ where κ is the average value of the curvature and δx is the space mesh size. Since we have volume conservation, the interface eventually becomes circular with constant curvature. Therefore, for given space mesh size δx, there is a δt threshold below which the interface will not move. Therefore time step refinement

beyond this threshold will not improve the accuracy of the interface position. However, when the interface intersects with the solid boundary, the motion of the contact point follows a different dynamics and is controlled by the Young stress $f = \gamma_{LV}(\cos\theta - \cos\theta_Y)$. This may lead to a different time scale (and a different time step constraint). Numerical results show that time step refinement improve the accuracy near the contact point. Hence, we propose an adaptive time step scheme to minimize the interfacial energy. The idea is that we first use a proper (large enough) time step δt so that the evolution of the interface reaches equilibrium state. We then improve the contact point accuracy by repeatedly halving the time step δt until the difference between the solutions of the successful step is less than a tolerance ε_1.

Modified Algorithm I

Step 0. *Given initial $D_1^0, D_2^0 \subset \Omega$, such that $D_1^0 \cap D_2^0 = \emptyset$, $D_1^0 \cup D_2^0 = \Omega$ and $|D_1^0| = V_0$. Set $D_1^* = D_1^0$. Set a tolerance parameter $\varepsilon > 0$.*

Step 1. *For given set (D_1^k, D_2^k), we define two functions*

$$\phi_1 = \frac{1}{\sqrt{\delta t}} G_{\delta t} * (\gamma_{LV}\chi_{D_2^k} + \gamma_{SL}\chi_{D_3}),\ \ \phi_2 = \frac{1}{\sqrt{\delta t}} G_{\delta t} * (\gamma_{LV}\chi_{D_1^k} + \gamma_{SV}\chi_{D_3}). \tag{29}$$

Step 2. *Find a constant δ by the fast scheme to keep volume conservation in the last subsection, so that the set*

$$\tilde{D}_1^\delta = \{x \in \Omega | \phi_1 < \phi_2 + \delta.\} \tag{30}$$

satisfying $|\tilde{D}_1^\delta| \approx V_0$. Denote $D_1^{k+1} = \tilde{D}_1^\delta$, $D_2^{k+1} = \Omega \setminus D_1^{k+1}$.

Step 3. *IF $|D_1^k - D_1^{k+1}| \le \varepsilon$,*
if $|D_1^* - D_1^{k+1}| \ge \varepsilon$,set $\delta t = \frac{\delta t}{2}$, $D_1^* = D_1^{k+1}$, and go back to step 1.
else, set $D_1^* = D_1^{k+1}$ and stop.
endif
ELSE, go back to step 1.
ENDIF

4.4. Accuracy check of the algorithms

To check the accuracy, we will apply the Modified Algorithm I described in Section 4.3 to a two-dimensional drop spreading on a solid surface. The equilibrium state is a circular arc with the Young's angle when the minimum

Table 1: Accuracy Check

Grid Points	L^1 Error	Convergence rate	L^1 Error with time refinement	Convergence rate
128× 128	0.1473	-	0.0515	–
256× 256	0.0482	2.06	0.0271	0.90
512× 512	0.0200	1.41	0.0109	1.49
1024 × 1024	0.0116	0.72	0.0054	1.02

of the total interfacial energy is reached. In our experiment, the initial liquid phase is given by a half circle centered at $(0, -\frac{\pi}{4})$ with the radius $\frac{\pi}{4}$. So the volume of the drop is $\frac{\pi^3}{32}$. We set three surface tensions as $\gamma_{LV} = 1, \gamma_{LS} = 1, \gamma_{SV} = 1 + \sqrt{3}/2$ which gives a Young's angle $\frac{\pi}{3}$. In this case, the exact equilibrium state can be computed explicitly.

In Fig.4, Fig.5 and Fig.6, we show the errors of computed solution (characteristic function) by both Algorithm I and the Modified Algorithm I, compared with the exact solution (the characteristic function of the exact equilibrium state) which shows location error of the interface. It is obvious that the errors near contact points are much larger than that at other places on the interfaces. However, after time step refinement, the Modified Algorithm 1 gives much improved results.

Then we check the accuracy of the modified version of Algorithm I via calculating the convergence rate of the L^1 error with respect to the refinement of the mesh. Table.1 shows L^1 errors of both schemes. Again the Modified Algorithm I gives much better results. The results also show that the convergence rate of our algorithm is of first order. Fig.7 gives very good comparison between the numerical solution and exact solution when it reaches equilibrium.

5. Droplet spreading on chemically pattern solid surface

We first study the hysteresis behavior of a drop spreading on a chemically patterned surface. We consider the quasi-static spreading of a droplet. To simulate the hysteresis process. we need to add or decrease the volume of the drop gradually. In each step, we need to compute the equilibrium state

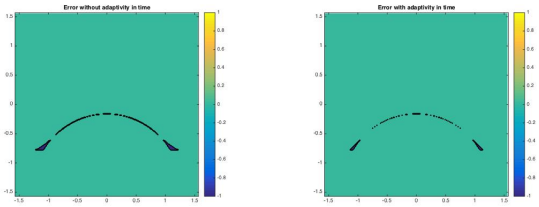

Figure 4: Left: 256 $\times$ 256 grid points, $\delta t = 2dx$ without adaptivity in time, Right:256 $\times$ 256 grid points, $\delta t = 2dx$ initially with adpativity in time, $\epsilon = 1.0e^{-10}$

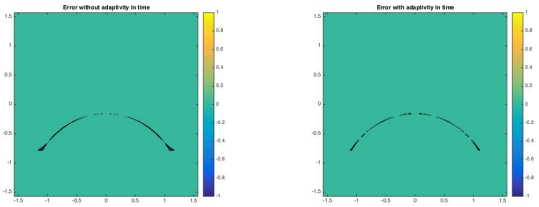

Figure 5: Left: 512 $\times$ 512 grid points, $\delta t = 2dx$ without adaptivity in time, Right:512 $\times$ 512 grid points, $\delta t = 2dx$ initially with adpativity in time, $\epsilon = 1.0e^{-10}$

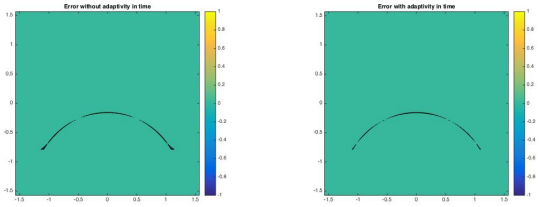

Figure 6: Left: 1024 $\times$ 1024 grid points, $\delta t = 2dx$ without adaptivity in time, Right:1024 $\times$ 1024 grid points, $\delta t = 2dx$ initially with adpativity in time, $\epsilon = 1.0e^{-10}$

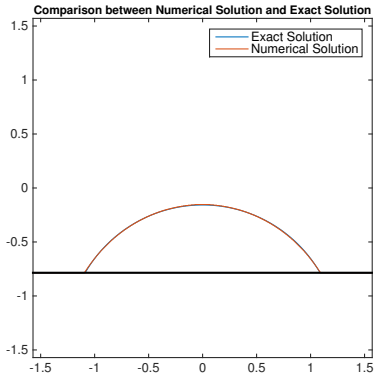

Figure 7: Red line represent the exact solution while the blue line represent the numerical solution(computed with 1024×1024 grid points). The static numerical solution is at the sense of the energy approaching the minimum and nothing changed when thresholding.

of the drop after liquid is added or extracted, which is very computationally demanding. We show that our threshold dynamics method can simulate the process efficiently.

We assume that the surface is periodically patterned in the interval $(-\pi/2, \pi/2)$ and the interval is divided into $2k+1$ periods with equal partition of two materials away from the center. The center part is occupied by the material $\mathcal{B}$ (See Fig.8). Assume $\theta_{\mathcal{A}}$, $\theta_{\mathcal{B}}$ are the Young's angle for material $\mathcal{A}$ and $\mathcal{B}$ respectively. r is the initial radius of a half circle on the surface and ΔV is the volume we add to the drop each time. In [32], the authors explicitly calculate the change of contact angle and position of contact points with respect to the volume for some simple two phase systems on the chemically patterned surface.

To implement the Modified Algorithem I, we need to divide our solid region into two parts (D_3, D_4) which represent material $\mathcal{A}$ and material $\mathcal{B}$ with different surface tensions, respectively (as shown in Figure 8) and modify the original $\gamma_{SL}\chi_{D_3}$, $\gamma_{SV}\chi_{D_3}$ into $\gamma_{S_1L}\chi_{D_3} + \gamma_{S_2L}\chi_{D_4}, \gamma_{S_1V}\chi_{D_3} + \gamma_{S_2V}\chi_{D_4}$. As the volume of the drop increases quasi-statically, we use the Modified Algorithem I to calculate the equilibrium state for each fixed volume.

We take $\theta_{\mathcal{A}} = \frac{\pi}{5}$, $\theta_{\mathcal{B}} = \frac{7\pi}{10}$. For the advancing drop, we plot the contact angle and position of contact point as functions of increasing volume in Fig.9 for $k = 2$ and in Fig.10 for $k = 4$. The contact point goes through the

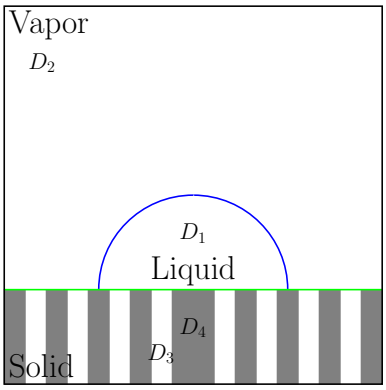

Figure 8: Diagrammatic sketch of the divide of the chemically patterned solid surface, this is a special case for $k = 4$. The yellow region is occupied by the material $\mathcal{B}$ while the blue region is occupied by $\mathcal{A}$.

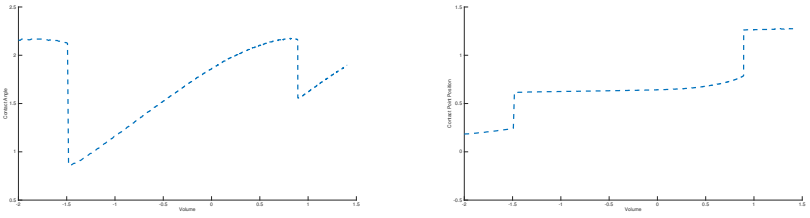

Figure 9: The stick-slip motion of a droplet with k=2 when the volume is increasing. $\theta_{\mathcal{A}} = \frac{\pi}{5}$, $\theta_{\mathcal{B}} = \frac{7\pi}{10}$.

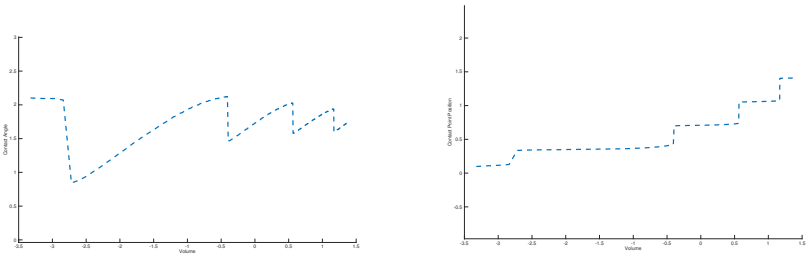

Figure 10: The stick-slip motion of a droplet with k=4 when the volume is increasing. $\theta_{\mathcal{A}} = \frac{\pi}{5}$, $\theta_{\mathcal{B}} = \frac{7\pi}{10}$.

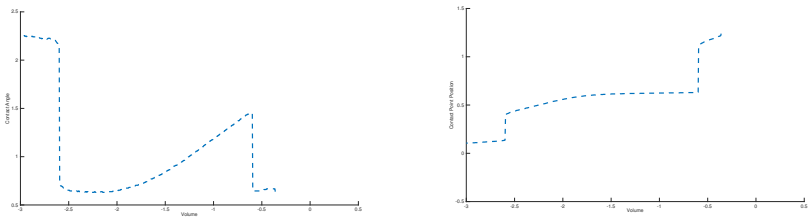

Figure 11: The stick-slip motion of a droplet with k=2 when the volume is decreasing. $\theta_{\mathcal{A}} = \frac{\pi}{5}$, $\theta_{\mathcal{B}} = \frac{7\pi}{10}$.

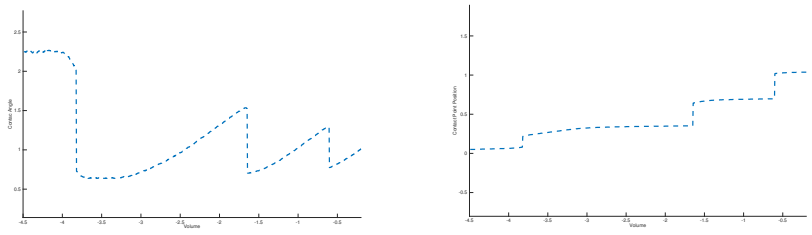

Figure 12: The stick-slip motion of a droplet with k=4 when the volume is decreasing. $\theta_{\mathcal{A}} = \frac{\pi}{5}$, $\theta_{\mathcal{B}} = \frac{7\pi}{10}$.

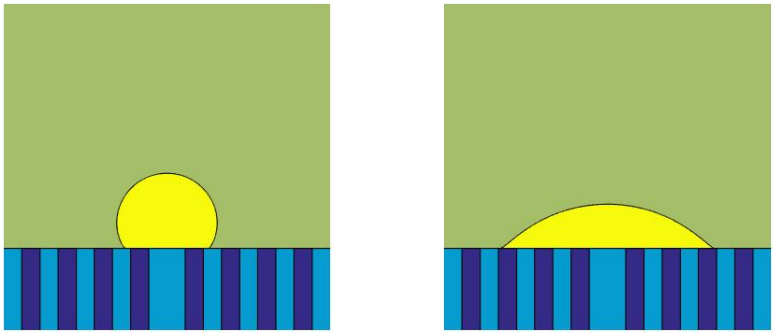

Figure 13: Left: The quasi-static state in the process of increasing the volume on chemically patterned surface when the volume is 0.5883. Right: The quasi-static state in the process of decreasing the volume on chemically patterned surface when the volume is 0.5883. The Young's angle on the light blue part is $\mathcal{B}$ while the Young's angle on the dark blue part is $\mathcal{A}$, k=4.

stick-slip motion, and the contact angle oscillates near the advancing angle $\theta_{\mathcal{B}}$ for larger k.

For the receeding drop, we plot the contact angle and position of contact point as functions of increasing volume in Fig.11 for $k = 2$ and in Fig.12 for $k = 4$. Again, the contact point goes through the stick-slip motion, but and the contact angle oscillates near the receding angle $\theta_{\mathcal{A}}$ for larger k.

In Fig. 13, we show two quasi-static drops. One is in the process of increasing the volume (advancing) and the other is in the process of decreasing volume (receding). We see that the two states have very different contact angles although they correspond to the same volume. This clearly shows the contact angle hysteresis as the shape of a droplet on a chemically patterned surface depends on its history.

6. Droplet spreading on a rough solid surface

In this part, we will simulate the contact angle hysteresis on a geometrically rough surface.

In our experiments, the computational domain is $[-\frac{\pi}{2}, \frac{\pi}{2}] \times [-\frac{\pi}{2}, \frac{\pi}{2}]$, then we take the solid surface as a sawtooth profile by an explicit function

$$y = -\frac{\pi}{4} + \tan(\alpha)\frac{\pi}{4k+2}|s((2k+1)x - \pi)|$$

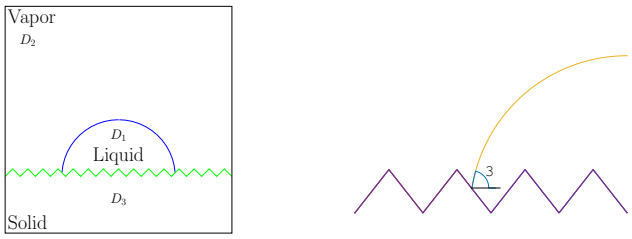

Figure 14: Left:Diagrammatic sketch of the rough solid surface, we take the solid surface as a sawtooth profile. Right: Diagrammatic sketch of effective contact angle θ on the rough solid surface.

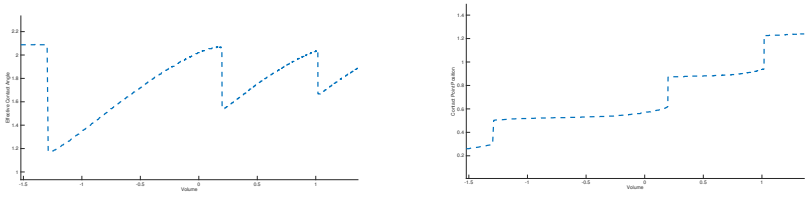

Figure 15: The stick-slip motion of a droplet on rough surface when the volume is increasing. $\theta = \frac{\pi}{2}, k = 4, \alpha = \frac{\pi}{6}$.

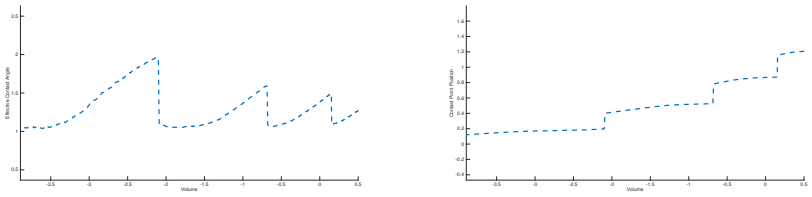

Figure 16: The stick-slip motion of a droplet on rough surface when the volume is decreasing. $\theta = \frac{\pi}{2}, k = 4, \alpha = \frac{\pi}{6}$.

where $s(x)$ is a sawtooth periodic function with period 2π define as

$$s(x) = \begin{cases} \frac{2}{\pi}(x+\pi) - 1 & -\pi \le x \le 0; \\ -\frac{2}{\pi}x + 1 & 0 \le x \le \pi. \end{cases}$$

For the rough surface, it is more meaningful to see the behavior of effective contact angle when increasing or decreasing the volume of the drop [7]. Where effective contact angle is defined by the angle between the contact line and the horizontal surface (See Fig. 14). Fig. 15 and Fig. 16 show the bahavior of the contact angle and the x-coordinate of contact point for the case $k = 4, \alpha = \frac{\pi}{6}$. The Young's angle of the solid surface is $\theta_Y = \frac{\pi}{2}$. We can see obvious stick-slip motion when we increase or decrease volume of the droplet. Furthermore, the advancing angle is almost $\frac{2\pi}{3}$ and the receding contact angle is about $\frac{\pi}{3}$.

In Figure 17, again, we show two quasi-static drops. One is in the process of increasing the volume (advancing) and the other is in the process of decreasing volume (receding). Similar to the chemically patterned surface case, we also see that the two states have very different apparent contact angles which corresponds to the contact angle hysteresis on rough surface.

Above simulations imply that our algorithm is not sensitive to the inhomogeneity or roughness of the solid boundary. The algorithm is quite stable, simple and efficient. This shows the great advantage of our algorithm when compared with solving a phase field model with relaxation boundary condition.

Acknowledgments

This publication was based on work supported in part by the Hong Kong RGC-GRF grants 605513, 16302715, RGC-CRF grant C6004-14G. XM Xu is also supported in part by NSFC 11571354

[1] G. Alberti and G. Bellettini. A non-local anisotropic model for phase transitions: asymptotic behaviour of rescaled energies. *Euro. J. Appl. Math.*, 9(03):261–284, 1998.

[2] G. Alberti and A. DeSimone. Wetting of rough surfaces: A homogenization approach. *Proc. R. Soc. A*, 451:79–97, 2005.

[3] G. Barles and C. Georgelin. A simple proof of convergence for an approximation scheme for computing motions by mean curvature. *SIAM J. Numer. Anal.*, 32(2):484–500, 1995.

Figure 17: Left: The quasi-static state in the process of increasing the volume on sawtooth rough surface when the volume is 1.178. Right: The quasi-static state in the process of decreasing the volume on sawtooth rough surface when the volume is 1.178. $\theta = \frac{\pi}{2}, k = 4, \alpha = \frac{\pi}{6}$.

[4] A. L. Bertozzi, S. Esedoglu, and A. Gillette. Inpainting of binary images using the cahn-hilliard equation. *IEEE Transactions on image processing*, 16(1):285–291, 2007.

[5] A. Cassie and S. Baxter. Wettability of porous surfaces. *Transactions of the Faraday Society*, 40:546–551, 1944.

[6] A. Chambolle and M. Novaga. Convergence of an algorithm for the anisotropic and crystalline mean curvature flow. *SIAM J. Math. Anal.*, 37(6):1978–1987, 2006.

[7] X. Chen, X.-P. Wang, and X. Xu. Effective contact angle for rough boundary. *Physica D: Nonlinear Phenomena*, 242(1):54–64, 2013.

[8] X. Chen, X.-P. Wang, and X. Xu. Analysis of the cahn-hilliard equation with relaxation boundary condition modelling contact angle. *Arch. Rational Mech. Anal.*, 213:1–24, 2014.

[9] P. de Gennes, F. Brochard-Wyart, and D. Quere. *Capillarity and Wetting Phenomena*. Springer Berlin, 2003.

[10] K. Deckelnick, G. Dziuk, and C. M. Elliott. Computation of geometric partial differential equations and mean curvature flow. *Acta numerica*, 14:139–232, 2005.

[11] C. M. Elliott and V. Styles. Computations of bidirectional grain boundary dynamics in thin metallic films. *Journal of Computational Physics*, 187(2):524–543, 2003.

[12] H. Y. Erbil. The debate on the dependence of apparent contact angles on drop contact area or three-phase contact line: a review. *Surface Science Reports*, 69(4):325–365, 2014.

[13] S. Esedoglu and F. Otto. Threshold dynamics for networks with arbitrary surface tensions. *Comm. Pure Appl. Math.*, 2015.

[14] S. Esedoglu, S. Ruuth, and R. Tsai. Threshold dynamics for high order geometric motions. *Interfaces and Free Boundaries*, 10(3):263–282, 2008.

[15] L. C. Evans. Convergence of an algorithm for mean curvature motion. *Indiana Math. J.*, 42(2):533–557, 1993.

[16] C. W. Extrand. Model for contact angles and hysteresis on rough and ultraphobic surfaces. *Langmuir*, 18:7991–7999, 2002.

[17] C. A. Hoare. Quicksort. *The Computer Journal*, 5(1):10–16, 1962.

[18] K. Ishii. Optimal rate of convergence of the bence–merriman–osher algorithm for motion by mean curvature. *SIAM J. Math. Anal.*, 37(3):841–866, 2005.

[19] C. Kublik, S. Esedoglu, and J. A. Fessler. Algorithms for area preserving flows. *SIAM J. Sci. Comput.*, 33(5):2382–2401, 2011.

[20] S. Leung and H. Zhao. A grid based particle method for moving interface problems. *Journal of Computational Physics*, 228(8):2993–3024, 2009.

[21] B. Merriman, J. K. Bence, and S. Osher. *Diffusion generated motion by mean curvature*. Department of Mathematics, University of California, Los Angeles, 1992.

[22] B. Merriman, J. K. Bence, and S. J. Osher. Motion of multiple junctions: A level set approach. *J. Comput. Phy.*, 112(2):334–363, 1994.

[23] M. Miranda, D. Pallara, F. Paronetto, and M. Preunkert. Short-time heat flow and functions of bounded variation in r^n. In *Annales-Faculte des Sciences Toulouse Mathematiques*, volume 16, page 125. Université Paul Sabatier, 2007.

[24] D. Quere. Wetting and roughness. *Annu. Rev. Mater. Res.*, 38:71–99, 2008.

[25] S. J. Ruuth. A diffusion-generated approach to multiphase motion. *J. Comput. Phy.*, 145(1):166–192, 1998.

[26] S. J. Ruuth. Efficient algorithms for diffusion-generated motion by mean curvature. *J. Comput. Phy.*, 144(2):603–625, 1998.

[27] S. J. Ruuth and B. T. Wetton. A simple scheme for volume-preserving motion by mean curvature. *J. Sci. Comput.*, 19(1-3):373–384, 2003.

[28] Y. Shi and X.-P. Wang. Modeling and simulation of dynamics of three-component flows on solid surface. *Japan Journal of Industrial and Applied Mathematics*, 31(3):611–631, 2014.

[29] R. N. Wenzel. Resistance of solid surfaces to wetting by water. *Ind. Eng. Chem.*, 28:988–994, 1936.

[30] G. Whyman, E. Bormashenko, and T. Stein. The rigorous derivative of young, cassie-baxter and wenzel equations and the analysis of the contact angle hysteresis phenomenon. *Chem. Phy. Letters*, 450:355–359, 2008.

[31] D. E. Womble. A front-tracking method for multiphase free boundary problems. *SIAM journal on numerical analysis*, 26(2):380–396, 1989.

[32] X. Xu and X. P. Wang. Analysis of wetting and contact angle hysteresis on chemically patterned surfaces. *SIAM J. Appl. Math.*, 71:1753–1779, 2011.

[33] X. Xu and X. P. Wang. The modified cassie's equation and contact angle hysteresis. *Colloid Polym. Sci.*, 291:299–306, 2013.

[34] T. Young. An essay on the cohesion of fluids. *Philos. Trans. R. Soc. London*, 95:65–87, 1805.

[35] H.-K. Zhao, T. Chan, B. Merriman, and S. Osher. A variational level set approach to multiphase motion. *J. Comput. Phy.*, 127(1):179–195, 1996.